ELSEVIER

14 October 1994

Chemical Physics Letters 228 (1994) 633–640

CHEMICAL PHYSICS LETTERS

Infrared emission spectroscopy at 100 μm. Vibration–rotation spectrum of CsI

V. Braun [a], B. Guo [a], K.-Q. Zhang [a], M. Dulick [a], P.F. Bernath [a], G.A. McRae [b]

[a] *Centre for Molecular Beams and Laser Chemistry, Department of Chemistry, University of Waterloo, Waterloo, Ontario, Canada N2L 3G1*

[b] *Atomic Energy of Canada Limited, Chalk River Nuclear Laboratories, Chalk River, Ontario, Canada K0J 1J0*

Received 3 May 1994; in final form 16 August 1994

Abstract

The vibration–rotation emission spectrum of CsI was recorded in the 110–130 cm^{-1} region of the spectrum. Although individual rotational lines were not resolved, we measured the positions of 29 band heads involving the vibrational bands from 1–0 to 30–29. These vibrational data when combined with previously measured microwave and millimeter-wave pure rotational transitions yielded improved Dunham constants. In addition, an experimentally derived Born–Oppenheimer potential is also reported and compared with the purely ionic internuclear potential of the Rittner model. The results reported here demonstrate that far-infrared emission spectroscopy is a very sensitive technique for detecting high-temperature molecules, even at wavelengths around 100 μm.

1. Introduction

Cesium iodide, a crystalline solid at room temperature, is an extremely volatile substance at elevated temperatures. Because of its volatility, attention recently has been directed toward CsI as a prime candidate in the transport of radioactive iodine from fission products produced in nuclear reactors [1].

Previous spectroscopic work on the alkali halides has included microwave absorption experiments. CsI is an ionic molecule with a large dipole moment of 11.69 D [2]. Pure rotational spectra have been obtained for most of the diatomic alkali halides in the centimeter-wave region [3,4], and for alkali bromides and iodides in the millimeter-wave region [5]. The hyperfine structure of CsI was measured for the $J=2\rightarrow3$ rotational transition by Hoeft et al. [6]. The most recent work was carried out by Honerjäger and Tischer [7], who obtained the rotational spectra of cesium halides in the 1 cm wavelength region and combined their results with the millimeter-wave data of Rusk and Gordy [5] to yield an improved set of Dunham Y constants.

Additional work included electron diffraction studies on CsI in the gas phase [8]. Oldenberg et al. [9] obtained the CsI ultraviolet chemiluminescence spectrum from the reaction Cs_2+I_2. Rounding out these type of investigations on CsI in the gas phase are photodissociation [10–12], collision-induced dissociation [13–17], and mass spectrometric [18–20] studies.

In contrast, only a limited amount of infrared spectroscopic work has been reported for CsI. The far-IR absorption spectrum of CsI isolated in solid argon has been reported [21]. Rice and Klemperer [22] measured IR spectra of several lighter alkali halides and performed an extrapolation to determine the vibrational frequency of CsI. Konings et al. [1] recorded

0009-2614/94/$07.00
SSDI 0009-2614(94)00998-8

a 0.1 cm^{-1} low-resolution IR absorption spectrum in the gas phase. They assigned the broad double-peaked feature, centered at 113.9 cm^{-1}, to the fundamental vibrational band of CsI but were unable to resolve any rotational structure.

In this Letter, we report on the analysis of the far-IR emission spectrum of CsI recorded with a Fourier transform spectrometer. Band head positions were measured consecutively from 1–0 to 30–29, with the exception of the 17–16 band which was not measured. The infrared data were then combined with pure rotational lines from the literature to yield improved spectroscopic constants for the $X\,^1\Sigma^+$ ground state.

2. Experimental

The experimental procedures followed were similar to those described in a previous paper on AlCl [23]. A 10 g sample of CsI was gradually heated to 900°C in a carbon boat placed in the center of a carbon liner that was housed inside of a Mullite ($3Al_2O_3 \cdot 2SiO_2$) tube. The tube was pressurized with 10 Torr of argon gas to prevent condensation of CsI on the polyethylene windows. The central 50 cm portion of the Mullite tube, 1.2 m in length and with an outside diameter of 5 cm, was heated by a commercial CM Rapid Temp furnace. The ends of the Mullite tube were water cooled and the window holders were attached with O rings.

The infrared radiation from the furnace was directed through the emission port of a Bruker IFS 120 HR Fourier transform spectrometer at the University of Waterloo. The far-IR emission spectrum was recorded with a liquid-helium cooled Si bolometer from Infrared Laboratories and a 12 μm Mylar beamsplitter.

At 900°C where the vapor pressure of CsI is estimated to be 30 Torr [24], 90 scans were coadded at a resolution of 0.01 cm^{-1} in the 50–200 cm^{-1} spectral range.

Fig. 1 shows a compressed view of the far-infrared emission spectrum of CsI. The sharp lines, labelled in Fig. 1 with leader lines, are actually rovibrational band heads where rotational lines from each vibrational band form heads at $J \approx 300$ in the R branch. The positions of 29 band heads were measured for the 1–0 to 30–29 bands, with the exception of 17–16, which was not measured due to the presence of a strong H_2O absorption band. Actual measurement of band head positions was accomplished by using Brault's computer program PC-DECOMP and proceeded by calibration with respect to impurity H_2O lines also present in the spectrum [25].

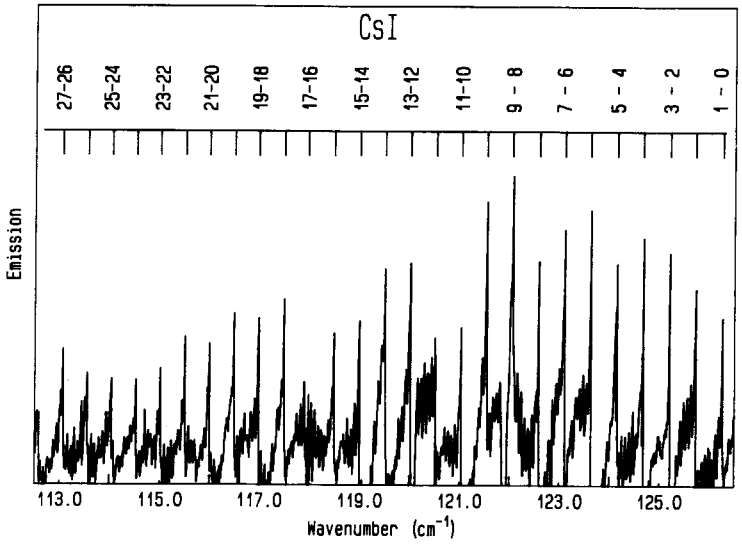

Fig. 1. A portion of the vibration–rotation emission spectrum of CsI with the band heads marked above.

Table 1
Pure rotational transitions of CsI (in cm^{-1})

v	$J' \leftarrow J''$	Observed	Obs. − calc. ($\times 10^{-7}$)
0	3←2	0.1415587 [a]	−9
0	16←15	0.7549309 [b]	52
0	17←16	0.8021016 [b]	13
0	18←17	0.8492719 [b]	−14
0	20←19	0.9436108 [c]	−36
0	104←103	4.8906551 [d]	−6
0	111←110	5.2173437 [d]	−10
0	128←127	6.0086465 [d]	10
0	135←134	6.3335389 [d]	9
0	139←138	6.5189272 [d]	13
1	3←2	0.1411499 [a]	−7
1	16←15	0.7527548 [b]	106
1	17←16	0.7997853 [b]	30
1	18←17	0.8468205 [b]	16
1	20←19	0.9408855 [c]	−17
1	111←110	5.2021936 [d]	−52
1	128←127	5.9911771 [d]	14
1	129←128	6.0374874 [d]	2
1	139←138	6.4999507 [d]	−19
2	3←2	0.1407419 [a]	−3
2	17←16	0.7974750 [b]	74
2	18←17	0.8443728 [b]	47
2	20←19	0.9381615 [c]	−27
2	111←110	5.1870788 [d]	39
2	128←127	5.9737340 [d]	27
2	139←138	6.4810056 [d]	−2
3	3←2	0.1403339 [a]	−4
3	17←16	0.7951658 [b]	93
3	20←19	0.9354428 [c]	−23
3	128←127	5.9563113 [d]	−12
3	140←139	6.5079926 [d]	−6
4	3←2	0.1399250 [a]	−20
4	20←19	0.9327278 [c]	−22
5	20←19	0.9300161 [c]	−29
6	20←19	0.9273111 [c]	−9
7	20←19	0.9246076 [c]	−16
8	20←19	0.9219096 [c]	−9
9	20←19	0.9192160 [c]	1
10	20←19	0.9165264 [c]	8
11	20←19	0.9138398 [c]	3
12	20←19	0.9111574 [c]	−4
13	20←19	0.9084881 [c]	7
14	20←19	0.9058086 [c]	15
15	20←19	0.9031394 [c]	12
16	20←19	0.9004728 [c]	−9
17	20←19	0.8978143 [c]	6
18	20←19	0.8954561 [c]	−20
19	20←19	0.8925062 [c]	−8
20	20←19	0.8898625 [c]	21
21	20←19	0.8872187 [c]	4
23	20←19	0.8819450 [c]	−28
24	20←19	0.8793212 [c]	17

[a] See text, Ref. [6]. [b] Ref. [3].
[c] See text, Ref. [7]. [d] Ref. [5].

3. Results and discussion

3.1. Dunham fits

All of the available microwave and millimeter-wave absorption data published so far on CsI [3,5–7] are displayed in Table 1. With the exception of the Hoeft et al. data [6], all of the reported data corresponds to pure rotational line frequencies with no resolved hyperfine structure. In order to incorporate the Hoeft et al. data set into our fits (where individual hyperfine lines for the $J=2\rightarrow 3$ transitions of $v=0$–3 were reported instead) line centers for these pure rotational transitions were calculated using their reported eqQ constants. A fit of the combined microwave and millimeter-wave data to the Dunham energy levels yielded a standard deviation of 0.675 with residuals given in Table 1.

The Dunham Ys obtained from this preliminary fit were then used in conjunction with the solutions of

$$\frac{\mathrm{d}}{\mathrm{d}J}\sum_{ij}(Y_{ij}(v+\tfrac{1}{2})^i\{[(J+1)(J+2)]^j - [J(J+1)]^j\})=0, \quad (1)$$

to obtain $\mathrm{R}(J)$ assignments for the band heads.

Two separate fits were then performed with a data set that combined the band head data with the microwave and millimeter-wave data. In the first fit, designated unconstrained, all Dunham Ys were treated as adjustable parameters. The second fit, designated constrained, involved treating the Y_{i0} and Y_{i1} as adjustable parameters and fixing all remaining Y_{ij} for $j>1$ to constraints imposed by the Dunham model [23,26]. The standard deviations for the unconstrained and constrained fits were 0.674 and 0.802, respectively. Other pertinent results from these fits reported here are the band head residuals from the constrained fit (Table 2) and the Dunham Y values along with their uncertainties quoted to 1 standard deviation (Table 3).

Previous Dunham constants reported by Honerjäger and Tischer are also listed in Table 3 for comparison purposes. Note that they also used Dunham relations similar to ours in determining the constants Y_{10}, Y_{20}, Y_{03}, and Y_{04}. Strictly speaking, the Dunham relation constraints are valid for only isotopically invariant Dunham U constants, i.e. constants that con-

Table 2
Band head position in cm^{-1}

Band	Band origin	Band head	Obs.−calc.
1–0	118.6587	126.2504	−0.0016
2–1	118.1630	125.7216	0.0007
3–2	117.6672	125.1928	0.0011
4–3	117.1711	124.6640	−0.0004
5–4	116.6827	124.1430	0.0041
6–5	116.1878	123.6157	0.0004
7–6	115.6975	123.0932	−0.0004
8–7	115.2109	122.5745	0.0007
9–8	114.7234	122.0551	−0.0007
10–9	114.2380	121.5380	−0.0018
11–10	113.7563	121.0248	−0.0008
12–11	113.2686	120.5057	−0.0075
13–12	112.7968	120.0027	−0.0001
14–13	112.3195	119.4943	0.0001
15–14	111.8435	118.9874	−0.0001
16–15	111.3706	118.4838	0.0011
18–17	110.4266	117.4788	0.0002
19–18	109.9552	116.9772	−0.0022
20–19	109.4915	116.4834	0.0014
21–20	109.0238	115.9858	−0.0008
22–21	108.5606	115.4929	−0.0001
23–22	108.0994	115.0021	0.0008
24–23	107.6389	114.5122	0.0008
25–24	107.1798	114.0239	0.0005
26–25	106.7247	113.5397	0.0024
27–26	106.2679	113.0540	0.0009
28–27	105.8107	112.5681	−0.0026
29–28	105.3587	112.0875	−0.0027
30–29	104.9127	111.6131	0.0016

The observed−calculated values correspond to residuals obtained from the combined fit of band heads, microwave, and millimeter-wave data to the Dunham model with constraints. Estimates of band origins are based on the parameters listed in the second column of Table 3.

vey information solely about the mechanical effects of nuclear motion with the reduced mass explicitly factored out. However, since

$$2B_e/\omega_e \approx 0.0004\,, \tag{2}$$

it can be safely assumed that Born–Oppenheimer breakdown, implicitly absorbed in the Ys and of order $2B_e/\omega_e$, is negligible. Therefore, applying these relations to the Ys is justified.

Finally, with the Y_{01} value obtained from the constrained fit along with the atomic masses taken from Mills et al. [27], we calculated the equilibrium internuclear separation R_e to be 3.31519042(40) Å.

3.2. Born–Oppenheimer potential

The results in Tables 2 and 3 are quite astonishing in view of the fact that the vibrational constants, Y_{10}, Y_{20}, and Y_{30}, were determined to such high degrees of precision from fits containing band head data. Moreover, the agreement between observed and calculated band head positions is in most cases considerably better than the assigned statistical weight of 0.002 cm^{-1}. Clearly the incorporation of microwave and millimeter-wave lines to the data set together with Dunham constraints enhance the precision of these constants. But the question remains as to whether this statistical information is providing a realistic estimate as to how accurate one can expect to predict $\Delta v = +1$ rotational line frequencies with these constants.

In contrast to the flexibility of the Dunham model, a more rigid model was also tried, similar to the one used in the analysis of AlF and AlCl [23]. Specifically, this involved fitting the data directly to the eigenvalues of the radial Schrödinger equation,

$$\left(\frac{\hbar^2}{2\mu}\nabla^2 - U^{BO}(R) + E(v,J) - \frac{\hbar^2}{2\mu}[1+q(R)]J(J+1)/R^2\right) \times \psi(r;v,J) = 0\,, \tag{3}$$

with the parameterized Born–Oppenheimer potential,

$$U^{BO} = D_e \frac{\{1-\exp[-\beta(R)]\}^2}{\{1-\exp[-\beta(\infty)]\}^2}\,, \tag{4}$$

where

$$\beta(R) = z\sum_{i=0}\beta_i z^i\,, \tag{5}$$

and

$$z = (R-R_e)/(R+R_e)\,. \tag{6}$$

Potential parameters obtained from this fit are displayed in Table 4 where the dissociation energy D_e was fixed to the value given in Ref. [28]. The standard deviation was now significantly higher, 60.4, with the largest increase in the residuals contributed by the band head data with a root-mean-square deviation of 0.197 cm^{-1}. It is also important to note that the statistical weights used in the Dunham Y fits,

Table 3
Dunham Y constants for CsI (in cm^{-1})

Constant	This work		Ref. [7]
	unconstrained	constrained [a]	
Y_{10}	119.16002(144)	119.165242(975)	119.1776(76)
Y_{20}	−0.250285(116)	−0.2505696(750)	−0.2505(7)
10^3Y_{30}	0.28453(293)	0.28573(197)	–
10^2Y_{01}	2.36274612(245)	2.36273842(58)	2.3627357(15)
10^3Y_{11}	−0.06827322(967)	−0.06826443(377)	−0.0682626(70)
10^6Y_{21}	0.048969(991)	0.048780(533)	0.04893(80)
10^9Y_{31}	0.1255(281)	0.1224(187)	0.114(25)
10^9Y_{02}	−3.72237(141)	−3.71541832	−3.71464(47)
$10^{12}Y_{12}$	−2.028(196)	−2.30881029	−2.30(50)
$10^{13}Y_{22}$	–	0.253353610	–
$10^{15}Y_{03}$	−0.0714(321)	−0.250428337	−0.25043(13)
$10^{19}Y_{13}$	–	−0.981502746	–
$10^{20}Y_{23}$	–	0.798064841	–
$10^{22}Y_{04}$	–	−0.889215827	−0.8876(17)
$10^{24}Y_{14}$	–	0.152376355	–
$10^{28}Y_{05}$	–	−0.257041566	–
$10^{31}Y_{15}$	–	0.820852269	–
$10^{35}Y_{06}$	–	−0.875800401	–
$10^{41}Y_{07}$	–	−0.315840421	–

[a] See text.

Table 4
Born–Oppenheimer potential parameters

D_e (cm^{-1})	28710
R_e (Å)	3.3150949(177)
β_0	4.404121(304)
β_1	−1.0409(190)

3×10^{-6} cm^{-1} for the microwave and millimeter-wave lines and 0.002 cm^{-1} for the band head positions, were also used in this fit. Therefore, a fit of the data to this more rigid model places a conservative upper limit of 0.2 cm^{-1} on the accuracy of predicted $\Delta v=+1$ rotational line positions.

In addition to representing the Born–Oppenheimer potential by Eq. (4), we also obtained the Dunham form by expanding Eq. (4) in a power series about $R=R_e$. The Dunham potential constants derived in this manner are given in Table 5. For the purpose of comparison, the as derived from the Ys of the constrained fit are also listed.

Table 5
Dunham potential constants

	BO potential	Dunham Ys
a_0 (cm^{-1})	149382(267)	150253(477)
a_1	−3.43841(452)	−3.4286(154)
a_2	8.0309(220)	7.624(110)
a_3	−15.5029(657)	−12.960(514)
a_4	26.508(153)	17.42(206)
a_5	−41.552(306)	−18.61(790)

3.3. Rittner model

One additional model that we used in analyzing the data was the Rittner potential,

$$U(R)=-e^2\left(\frac{1}{R}+\frac{(\alpha_++\alpha_-)}{2R^4}+\frac{2\alpha_+\alpha_-}{R^7}\right)$$
$$-\frac{C_6}{R^6}+A\exp(-R/\rho)+U_0\,. \qquad (7)$$

In Eq. (7) α_+ and α_- are the atomic polarizabilities for Cs^+ and I^-, C_6 is a measure of the van der Waals attraction between ions, A and ρ are constants that

Table 6
Rittner parameters and potential constants

	BO potential		Dunham Y	
	B–K	S–A	B–K	S–A
α_+ (Å^3)	2.880	2.935	2.880	2.935
α_- (Å^3)	5.866	5.409	5.866	5.409
$10^5 C_6$ (cm^{-1} Å^6)	5.579	5.242	5.579	5.242
$10^7 A$ (cm^{-1})	3.785	3.886	3.882	3.989
ρ (Å)	0.3861	0.3836	0.3848	0.3823
R_e (Å)	3.3150949		3.31519042	
r_0 (cm^{-1})	149382		150253	
r_1	−3.530	−3.551	−3.543	−3.564
r_2	7.877	7.991	7.940	8.054
r_3	−13.11	−13.46	−13.28	−13.63
r_4	16.90	17.68	17.25	18.03
r_5	−16.19	−17.63	−16.75	−18.20

Table 7
Rittner Y constants in cm^{-1}

Y_{10}	119.165
Y_{20}	−0.2758
$10^4 Y_{30}$	2.981
$10^2 Y_{01}$	2.36273842
$10^5 Y_{11}$	−7.176
$10^8 Y_{21}$	3.268
$10^{10} Y_{31}$	2.388
$10^9 Y_{02}$	−3.715
$10^{12} Y_{12}$	−5.176
$10^{14} Y_{22}$	2.559
$10^{16} Y_{03}$	−3.231
$10^{18} Y_{13}$	−1.403
$10^{20} Y_{23}$	1.821
$10^{22} Y_{04}$	−1.313
$10^{25} Y_{14}$	−3.775
$10^{29} Y_{05}$	−4.992
$10^{33} Y_{15}$	1.366
$10^{35} Y_{06}$	−2.210
$10^{41} Y_{07}$	−1.014

correspond to the Born–Mayer form for repulsion, and U_0 is the dissociation energy [29].

A particular form of the Rittner potential conducive to the analysis of spectroscopic data is the power series expansion [3],

$$U(\xi)=U(0)+r_0\xi^2(1+r_1\xi+r_2\xi^2+r_3\xi^3+\ldots), \quad (8)$$

where

$$\xi\equiv(R-R_e)/R_e \quad (9)$$

and the minimum of $U(\xi)$ is constrained to lie at $\xi=0$.

By equating r_0 to the Dunham a_0, the remaining r_i are only functions of the Rittner parameters and R_e. Expressions for r_i have already been given by Honig et al. [3] and, therefore, are not reproduced here.

In the process of calculating r_i, Brumer–Karplus [30] and Shanker–Agrawal [31] polarizabilities for Cs^+ and I^- were chosen as representative values [32], while C_6 was estimated using London's formula [30],

$$C_6=-\frac{3}{2}\frac{I_{Cs}I_I}{I_{Cs}+I_I}\alpha_+\alpha_-, \quad (10)$$

where I_{Cs} is the ionization energy of atomic Cs, 3.893 eV [33], and I_I is the electron affinity of iodine, 3.063 eV [34]. The A and ρ repulsion constants were obtained by numerically solving

$$\left(\frac{dU(\xi)}{d\xi}\right)_{\xi=0}=0 \quad (11)$$

and

$$\left(\frac{d^2U(\xi)}{d\xi^2}\right)_{\xi=0}=2a_0. \quad (12)$$

Values of Rittner parameters and r_i calculated from B–K and S–A polarizabilities are tabulated in Table 6.

Comparison of a_i in Table 5 with r_i in Table 6 in-

dicates excellent agreement between the r_i and a_i obtained from the Dunham Ys. On the other hand, for a_i from the potential fit, good agreement is exhibited only between the lowest r_i and a_i and becomes progressively worse for the higher r_i and a_i.

The fact that a_i from the Dunham Ys rather than a_i from the potential fit agree with the Rittner r_i to $\leqslant 5\%$ seems to signify that the Rittner model is capable of predicting the spectrum much more accurately than the Born–Oppenheimer potential given by Eq. (4). To demonstrate that this was not the case, a set of Ys was computed by averaging the Rittner r_i appearing in the last two columns of Table 6. Generating a spectrum with these Rittner Ys (Table 7) gave a root-mean-square deviation of 1.2 cm^{-1} for the observed – calculated band-head positions (0.002 cm^{-1} for pure rotation transitions) as compared to 0.2 cm^{-1} for the Born–Oppenheimer potential fit. Thus, it appears that the Rittner model is capable of predicting the rovibrational spectrum to no better than ≈ 1 cm^{-1}. Obviously, a more refined treatment must await the analysis of resolved rotational structure in the far-IR spectrum before any final conclusion can be reached.

4. Conclusion

Infrared emission spectroscopy is a remarkably sensitive technique for the detection of high-temperature molecules, even at the longer wavelength end of the spectrum (100 μm). Although individual rotational lines could not be resolved because of the small rotational constant, $B \approx 0.02$ cm^{-1}, it was still possible to improve the vibrational constants by using band-head positions. The availability of high-precision microwave and millimeter-wave data allowed the separation between the band heads and band origins to be calculated reliably for the first time. Emission spectroscopy at very long wavelengths is not only feasible but is also a useful technique for elucidating molecular structure and monitoring the concentrations of molecules at high temperatures.

Acknowledgement

We wish to thank R. Honerjäger and T. Törring for providing the measured line positions used in Ref. [7]. We also wish to thank J. Ogilvie for kindly providing us with the Dunham relations in advance of publication. This work was supported by CANDU Owners Group Research and Development Program (WP8 WPIR 1807), AECL, and the Natural Science and Engineering Research Council of Canada.

References

[1] R.J.M. Konings, A.S. Booij and E.H.P. Cordfunke, Vib. Spectry. 2 (1991) 251.
[2] T.L. Story Jr. and A.J. Hebert, J. Chem. Phys. 64 (1976) 855.
[3] A. Honig, M. Mandel, M.L. Stitch and C.H. Townes, Phys. Rev. 96 (1954) 629.
[4] A. Honig, M.L. Stitch and M. Mandel, Phys. Rev. 92 (1953) 901.
[5] J.R. Rusk and W. Gordy, Phys. Rev. 127 (1962) 817.
[6] J. Hoeft, E. Tiemann and T. Törring, Z. Naturforsch. 27a (1972) 1017.
[7] R. Honerjäger and R. Tischer, Z. Naturforsch. 29a (1974) 819.
[8] J.G. Hartley and M. Fink, J. Chem. Phys. 89 (1988) 6053.
[9] R.C. Oldenberg, J.L. Gole and R.N. Zare, J. Chem. Phys. 60 (1974) 4032.
[10] J. Berkowitz, J. Chem. Phys. 50 (1969) 3503.
[11] W.R. Anderson, B.M. Wilson, R.C. Ormerod and T.L. Rose, J. Chem. Phys. 74 (1981) 3295.
[12] T.R. Su and S.J. Riley, J. Chem. Phys. 71 (1979) 3194.
[13] F.P. Tully, Y.T. Lee and R.S. Berry, Chem. Phys. Letters 9 (1971) 80.
[14] E.K. Parks and S. Wexler, J. Phys. Chem. 88 (1984) 4492.
[15] E.K. Parks, L.G. Pobo and S. Wexler, J. Chem. Phys. 80 (1984) 5003.
[16] E.K. Parks, M. Inoue and S. Wexler, J. Chem. Phys. 76 (1982) 1357.
[17] R. Milstein and R.S. Berry, J. Chem. Phys. 80 (1984) 6025.
[18] M.D. Scheer and J. Fine, J. Chem. Phys. 36 (1961) 1647.
[19] L. Brewer, Chem. Rev. 61 (1961) 425.
[20] R. Viswanathan and K. Hilpert, Phys. Chem. 88 (1984) 125.
[21] T.P. Martin and H. Schaber, J. Chem. Phys. 68 (1978) 4299.
[22] S.A. Rice and W. Klemperer, J. Chem. Phys. 27 (1957) 573.
[23] H.G. Hedderich, M. Dulick and P.F. Bernath, J. Chem. Phys. 99 (1993) 8363.
[24] O. Knacke, O. Kubaschewski and K. Hesselmann, Thermochemical properties of inorganic substances, 2nd ed. (Springer, Berlin, 1991).
[25] J.W.C. Johns, J. Opt. Soc. Am. B 2 (1985) 1340.
[26] J.L. Dunham, Phys. Rev. 41 (1932) 721.
[27] I. Mills, T. Cvitaš, K. Homann, N. Kallay and K. Kuchitsu, Quantities, units and symbols in physical chemistry (Blackwell, Oxford, 1988).

[28] K.P. Huber and G. Herzberg, Constants of diatomic molecules (Van Nostrand-Reinhold, New York, 1979).
[29] E. Rittner, J. Chem. Phys. 19 (1951) 1030.
[30] P. Brumer and M. Karplus, J. Chem. Phys. 58 (1973) 3903.
[31] J. Shanker and H.B. Agrawal, Can. J. Phys. 58 (1980) 950.
[32] J.E. Szymanski and J.A.D. Matthew, Can. J. Phys. 62 (1984) 583.
[33] C.E. Moore, Atomic energy levels, NSRDS-NBS Circular No. 35, Vol. 3 (US GPO, Washington, 1971).
[34] R.S. Berry and C.W. Reimann, J. Chem. Phys. 38 (1963) 1540.